Optimization of Pelvic Rotation Walking Pattern Considering Future States Using Model Predictive Control to Increase the Step Length

BEOMYEONG PARK[1] AND JAEHEUNG PARK[2,3], (Member, IEEE)

[1]Department of Transdisciplinary Studies, Graduate of School of Convergence Science and Technology, Seoul National University, Seoul 08826, South Korea
[2]Graduate School of Convergence Science and Technology, ASRI, RICS, Seoul National University, Seoul 08826, South Korea
[3]Advanced Institutes of Convergence Technology, Suwon 443-270, South Korea

Corresponding author: Jaeheung Park (park73@snu.ac.kr)

ABSTRACT Pelvic rotation, which is observed in human gait, is used to increase a robot's step length in the humanoid robot walking. Existing methods empirically or experimentally generate the pelvic-rotation angle offline using predetermined pelvis and foot trajectories. Therefore, these methods are difficult to be used with the method to generate the center of mass (CoM) trajectory in real time using techniques such as preview control or model predictive model control. In this study, we propose a method that generates a pelvic-rotation trajectory that can be used with a real-time CoM generation method while reflecting the future state of the robot. The step length increased due to pelvic rotation was kinematically analyzed and compared with the step length increased by the proposed method. Upper body motion to compensate for yaw angular momentum generated by lower body movement during walking using pelvic rotation was optimized using centroial dynamics. The waist yaw joint for pelvic rotation, leg joint for the walking, and upper body joint for arm swing were optimized using separate optimal controllers. Energy efficiency, increase in step length, and decrease in the possibility of singularity occurrence of pelvic rotation walking were analyzed and compared in simulations. The proposed method was experimentally verified using humanoid robot Dyros-Jet.

INDEX TERMS Humanoid robot, locomotion, trajectory optimization, model predictive control, quadratic programming.

I. INTRODUCTION

Humanoid robots have been studied for the purpose of being applied to human work environments. However, the low walking speed of humanoid robots limits their usability. Methods that enable long strides are required to improve the walking velocity of humanoid robots. Humanoid walking using pelvic rotation has been studied to increase step length. Pelvic rotation during walking causes the hip of the swing leg to move forward as the swinging foot moves. This movement increases the landing distance with respect to the pelvis length. A human gait analysis showed that pelvic rotation is also present in the human gait [1], [2]. The angular momentum generated during walking may weaken the stability of a robot because a longer the stride increases

The associate editor coordinating the review of this manuscript and approving it for publication was Jingang Jiang.

the yaw angular momentum generated by the swing of the leg. Biomechanics studies have revealed that humans use arm swings to compensate for the yaw angular momentum [3], [4]

The application of pelvic rotation to robot walking has been attempted to increase step length. In pelvic rotation walking, as the pelvis rotates, the hip of the swinging leg moves further forward than the hip of the supporting leg, and the step length can be increased. The yaw joint trajectory used for the pelvic rotation was determined offline using the previously generated pelvis and foot trajectories. A method used to generate the pelvic trajectory utilizes a sine function such that the pelvis can rotate according to the swing of the leg [2]. The pelvic rotation angle was experimentally determined to be proportional to the distance between the supporting and the swinging feet [5]. Additionally, the pelvic rotation angle was determined with respect to the velocity of the swinging foot [6]. Human walking motion data measured

by a motion-capture device were used to optimize the pelvic rotation walking pattern [7] to reduce the error between the robot and motion-capture date. A genetic algorithm was also used to optimize the pelvis and foot trajectories [8].

The aforementioned methods to determine the pelvic rotation angle are limited because both the pelvis and foot trajectories must be generated in advance. Therefore, the pelvic-rotation trajectory is not generated in real time. However, preview control or model predictive control (MPC), which is often used in humanoid robot walking research, generates a center of mass (CoM) trajectory in real time [9]–[12], which is difficult to combine with the method of generating the pelvic rotation trajectory introduced above. In a position-controlled robot, inverse kinematics (IK) was used to generate the angle of the leg joints using the positions and rotation trajectories of the pelvis and foot. To use IK, the pelvis and foot trajectories should be expressed in the same frame. For computational convenience, pelvis and foot trajectories that are expressed based on the pelvis frame are typically used for IK. Therefore, if the orientation of the pelvic-rotation trajectory is non-zero, the foot trajectory is generated by considering the rotation of the pelvis.

A method using the torso was proposed to compensate the yaw angular momentum of humanoid robot walking [13]–[16]. Using a simplified model of the robot's upper body generates the waist yaw joint trajectory required to rotate the torso. When the waist yaw joint is used to rotate the torso of the robot to compensate for the angular momentum, it cannot be used to increase the step length because the pelvic rotation is fixed. When walking using pelvic rotation, angular momentum cannot be compensated using the waist yaw joint; therefore, the robot arm should be used. To compensate for the yaw angular momentum using the robot's arm, a more accurate model than the simplified model of the robot's upper body is required. Centroidal dynamics, which calculate the momentum in the CoM frame, is used to generate the arm-swing motion of the robot [17], [18]. Centroidal dynamics can calculate the momentum generated by the movement of each joint of the robot; therefore, it can calculate momentum more accurately than a simplified model. Centroidal dynamics was used as the whole body controllers for balancing. Centroidal dynamics has also been used to generate upper-body movements to compensate angular momentum during walking [18]–[20].

Our previous study proposed a whole-body walking pattern generation method for the long step lengths. In the proposed method, the pelvic rotation trajectory was generated using the redundancy, and the method could be used with the real-time CoM trajectory generation method [21]. The lower body of the robot consisted of a waist yaw joint and both leg joints; therefore, it could be considered a redundant system. In addition, using the quadratic programming-based IK (QP-based IK) eliminated the process of changing the reference frame of the foot trajectory by reflecting the rotation of the pelvis. However, the future states of the foot and pelvis were not reflected; only the current states were
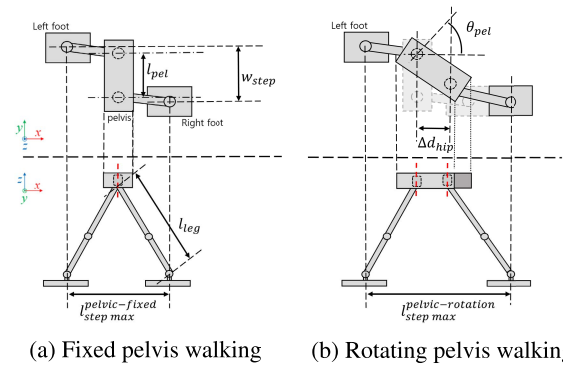

(a) Fixed pelvis walking   (b) Rotating pelvis walking

FIGURE 1. Kinematic analysis of pelvic rotation. Each figure shows the $x - y$ view at the top and $x - z$ view at the bottom.

reflected. Therefore, the waist yaw joint rotated only when the foot swung, and the angular velocity of the waist yaw joint increased rapidly as the step length increased. This sharp increase in the angular velocity of the waist joint may weaken the walking stability.

In this study, we propose a method to optimize the pelvic-rotation trajectory for a long step length by reflecting the future state of the robot. The MPC scheme optimizes the pelvic-rotation trajectory using the predicted future CoM positions and the pre-determined foot trajectory in advance. Using a redundant kinematic structure, in which the waist yaw joint is included in the lower body, the angles of the lower-body joints are obtained using the QP-based IK. By using a redundant lower body, it is unnecessary to change the frame of the foot trajectory to account for pelvic rotation. The effect of pelvic rotation on the increase in step length was kinematically analyzed and comparatively verified in simulations. In addition, the waist yaw joint cannot be used to compensate for the yaw angular momentum; therefore, an arm swing motion that compensates for the yaw angular momentum was generated using centroidal dynamics.

The remainder of this paper is organized as follows. Section II analyzes the effect of pelvic rotation on the increase in step length. The structure of the proposed system is explained in Section III. Section IV explains the concept of walking pattern generation. Section V describes the process of optimizing the walking pattern, including the pelvic rotation trajectory, using an MPC scheme. In Section VI, the results of the simulation and experiments are discussed, and Section VII concludes the paper.

II. KINEMATIC ANALYSIS

This section kinematically analyzes the extent to which pelvic rotation walking can increase step length. Fig. 1 shows the maximum step length with and without pelvic rotation. For the kinematic analysis of the increase in step length, it is assumed that the robot's left and right legs are outstretched, and the center of the pelvis is between the feet, as shown in Fig. 1. If the length of the leg when the knee is extended is l_{leg} and the height from the ankle to the hip joint is z_0, the maximum step length during walking without pelvic rotation,

(a) Fixed pelvis walking   (b) Rotating pelvis walking
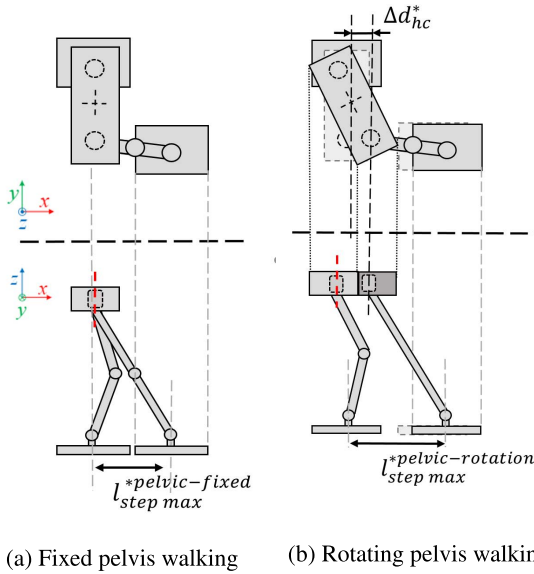
FIGURE 2. Kinematic analysis of step length when the foot lands. Each figure shows the $x-y$ view at the top and $x-z$ view at the bottom.

$l_{stepmax}^{pelvic-fixed}$ is as follows:

$$l_{stepmax}^{pelvic-fixed} = 2\sqrt{l_{leg}^2 - z_0^2}. \qquad (1)$$

When the pelvis rotates around the hip joint of the supporting leg by θ_{pel}, the forward distance in the sagittal plane between both hip joints, δd_{hip}, increases proportionalyy to the width of the pelvis and θ_{pel}:

$$\Delta d_{hip} = l_{pel} \cdot sin\theta_{pel}. \qquad (2)$$

The kinematically possible maximum step length during walking using pelvic rotation is when the line passing through both hip joints coincides with the line passing through the ankles of feet, and can be calculated using the length of the pelvis and the width between the feet.

$$l_{stepmax}^{pelvic-rotation} = \sqrt{(l_{max}^{step} + l_{pel})^2 - w_{step}^2} \qquad (3)$$

For kinematic analysis, it is assumed that the robot stands while the center of the pelvis is located between the feet with both legs extended. However, when the pelvis moves toward the front foot during the double support phase (DSP), a singularity occurs in the hind leg. Therefore, $l_{stepmax}^{pelvic-rotation}$ cannot be regarded as a possible step length for humanoid robot walking.

As a simple example, an increase in the step length owing to the pelvic rotation during static walking is shown in Fig. 2. During the single support phase (SSP), if it is assumed that the center of the pelvis is at the center of the supporting foot, and the robot does not fall, even during the leg swing. At this time, the maximum step length when walking without pelvic rotation is the distance from the hip to the ankle of the robot when the foot lands on the ground, and the knee of the swinging leg is fully extended.

$$l_{stepmax}^{*pelvic-fixed} = \sqrt{l_{leg}^2 - z_0^2}, \qquad (4)$$

Walking using pelvic rotation increased the step length in accordance with the angle of the pelvic rotation.

$$l_{stepmax}^{*pelvic-rotation} = \sqrt{l_{leg}^2 - z_0^2} + \Delta d_{hc}^*, \qquad (5)$$

where Δd_{hc}^* is the length from the left hip joint to the center of the pelvis in the x direction, ($\Delta d_{hc}^* = 0.5 * l_{pel} \cdot sin\theta_{pel}$). The humanoid robot used in this study, Dyros-Jet, had l_{leg} of 0.75 m, z_0 of 0.68 m, l_{pel} of 0.21 m, and w_{step} of 0.243 m. For the pelvic rotation angle, it is assumed that the hip joint of the right leg is sufficiently rotated to be in the same position as the ankle joint in the x direction. At this time, the pelvic rotation angle, $\theta_{pel} = 45°$, and the maximum step length with pelvic rotation is 0.42 m. The step length increased by 35% compared with the maximum step length of 0.31 m when walking without pelvic rotation.

III. OVERALL SYSTEM STRUCTURE
A. CONTROL FRAMEWORK STRUCTURE
Fig. 3 shows the overall control framework for pelvic rotation walking using the MPC scheme. The framework includes a walking pattern generator and a multi-layered optimal controller. In the walking pattern generator, a reference zero momentum point (ZMP) trajectory is generated using footholds created during footstep planning. The desired CoM trajectory is generated using an MPC [12] and desired base-frame trajectory is generated to track the CoM trajectory. The desired foot trajectory is generated such that the foot can move between the footholds.

The joint values input to the robot for pelvic-rotation walking were generated by dividing the joints into three parts: waist yaw joint, leg joints, and arm joints. In the order listed, the previously generated joint angles affect subsequent joint angles, but not vice versa. The multi-layered optimal controller consists of an MPC to optimize the pelvic-rotation trajectory, a QP-based IK for the lower body to track the desired foot trajectory, and a QP to generate upper body motion to compensate the yaw angular momentum. The predicted CoM trajectory and predefined foot trajectory are used in the MPC to optimize pelvic rotation. The waist-yaw-joint angular velocity of the pelvic rotation is optimized using the MPC scheme. The optimized waist-yaw-joint angular velocity is used as a constraint in the QP-based IK which is further used to optimize the joint angular velocity of the legs for the walking. The optimized angular velocities of the lower body joints in the previous two layers are used to calculate the yaw angular momentum of the lower body, which is then used for the cost function in the QP to compensate the momentum.

B. ROBOT SYSTEM KINEMATIC STRUCTURE
To generate the pelvic rotation trajectory in real time and not change the frame of the foot trajectory to reflect the pelvic rotation, the lower body is considered to be a redundant system by including the waist yaw joint, as shown in Fig. 4. The upper-body joints, $\mathbf{q}_{up}$, and lower body joints, $\mathbf{q}_{low}$ are
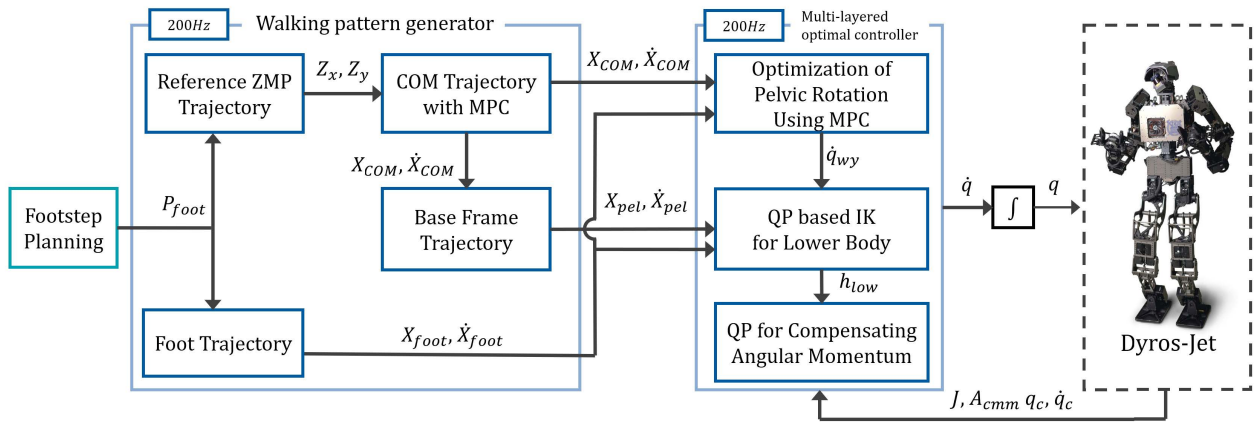
FIGURE 3. Proposed multi-layered control framework.

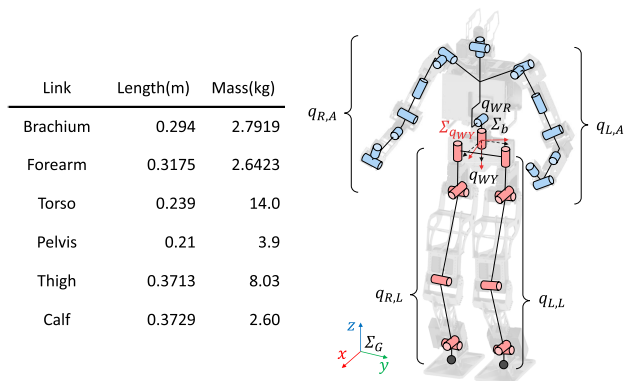| Link	Length(m)	Mass(kg)
Brachium	0.294	2.7919
Forearm	0.3175	2.6423
Torso	0.239	14.0
Pelvis	0.21	3.9
Thigh	0.3713	8.03
Calf	0.3729	2.60

FIGURE 4. Kinematic structure of the robot and the corresponding kinematic information of each link. The red and blue joints constitute the lower and upper body, respectively.

composed of 15 and 13 DoF, respectively:

$$\mathbf{q}_{low} = \begin{bmatrix} q_{WY} & \mathbf{q}_{LL} & \mathbf{q}_{RL} \end{bmatrix}^T, \tag{6}$$

$$\mathbf{q}_{up} = \begin{bmatrix} q_{WR} & \mathbf{q}_{LA} & \mathbf{q}_{RA} \end{bmatrix}^T. \tag{7}$$

In pelvic rotation walking, the angles of the leg joints used to track the walking task are affected by rotation of the pelvis. To reflect the pelvic rotation angle in the process of calculating the angle of the leg joints, the Jacobian of each leg is configured as follows.

$$\mathbf{J}_f = \begin{bmatrix} \mathbf{J}_{f,0} & \mathbf{J}_{f,1} & \mathbf{J}_{f,2} & \mathbf{J}_{f,3} & \mathbf{J}_{f,4} & \mathbf{J}_{f,5} & \mathbf{J}_{f,6} \end{bmatrix}, \tag{8}$$

where $\mathbf{J}_{f,j} \in \mathbb{R}^{6 \times 7}$ is the Jacobian matrix of one leg, and $\mathbf{J}_{f,j} \in \mathbb{R}^6$ is the foot Jacobian vector of joint j expressed in the pelvis-frame coordinate, respectively. $j = 0$ is the waist yaw joint and $j = 1, \ldots, 6$ are leg joints from the hip to the ankle. The lower body Jacobian is expressed as follows,

$$\mathbf{J}_{low} = \begin{bmatrix} \mathbf{J}_{Lf,0} & \mathbf{J}_{Lf,1-6} & 0 \\ \mathbf{J}_{Rf,0} & 0 & \mathbf{J}_{Rf,1-6} \end{bmatrix}, \tag{9}$$

where $\mathbf{J}_{low} \in \mathbb{R}^{12 \times 13}$ denotes the Jacobian matrix of the lower body. J_{Lf} and J_{Rf} are the left foot and right foot

Jacobian matrices expressed in the pelvis-frame coordinates, respectively.

IV. WALKING PATTERN GENERATION

This section describes the generation of the walking patterns. The CoM, pelvis, and foot trajectory are generated based on the supporting foot frame and are used after changing to the pelvis frame. In addition, the lower-body Jacobian that is expressed based on the pelvis frame is used in the structure of the robot system.

A. CoM TRAJECTORY GENERATION

In this study, a method that generates the CoM trajectory with minimal velocity fluctuation [12] is used for the humanoid robot walking. The method used to generate the CoM trajectory using the MPC scheme is briefly described, and the notation introduced in the study [12] is used. The height in the Z-direction of the CoM trajectory, z_c, is constant, and the position, velocity, and acceleration in the x and y-directions of the CoM are defined as states as follows:

$$\mathbf{x}_i = [x(t_i), \dot{x}(t_i), \ddot{x}(t_i)]^T, \tag{10}$$

$$\mathbf{y}_i = [y(t_i), \dot{y}(t_i), \ddot{y}(t_i)]^T, \tag{11}$$

$$\mathbf{x}_{i+1} = \mathbf{A}\mathbf{x}_i + \mathbf{B}\dddot{x}_i, \tag{12}$$

$$\mathbf{y}_{i+1} = \mathbf{A}\mathbf{y}_i + \mathbf{B}\dddot{y}_i. \tag{13}$$

The ZMP is defined as follows using the above equations and linear inverted pendulum model (LIPM) dynamics:

$$z_{x,i} = \mathbf{C}\mathbf{A}\mathbf{x}_i, \tag{14}$$

$$z_{y,i} = \mathbf{C}\mathbf{A}\mathbf{y}_i. \tag{15}$$

The N predictive ZMP states in the time horizon can be obtained by successively calculating (12)-(15)

$$\mathbf{Z}_{x,i+1} = [z_{x,i}, z_{x,i+1}, \ldots, z_{x,i+N-1}, z_{x,i+N}]^T, \tag{16}$$

$$\mathbf{Z}_{y,i+1} = [z_{y,i}, z_{y,i+1}, \ldots, z_{y,i+N-1}, z_{y,i+N}]^T. \tag{17}$$

The MPC scheme that uses the following objective function reduces the error with the pre-generated ZMP reference

introduced in Section III, which then reduces the CoM velocity fluctuation, and regularizes the CoM jerk.

$$\min_{\mathbf{U}_{x,i},\mathbf{U}_{y,i}} \quad \frac{\alpha_x}{2}\|\mathbf{Z}_{x,i} - \mathbf{Z}_{x,i}^{ref}\|^2 + \frac{\beta_x}{2}\|\Delta\mathbf{V}_{x,i}\|^2 + \frac{\gamma_x}{2}\|\mathbf{U}_{x,i}\|^2$$
$$+ \frac{\alpha_y}{2}\|\mathbf{Z}_{y,i} - \mathbf{Z}_{y,i}^{ref}\|^2 + \frac{\beta_y}{2}\|\Delta\mathbf{V}_{y,i}\|^2 + \frac{\gamma_y}{2}\|\mathbf{U}_{y,i}\|^2$$
$$\text{s.t.} \quad \mathbf{Z}_{x,i}^{min} \leq \mathbf{Z}_{x,i} \leq \mathbf{Z}_{x,i}^{max},$$
$$\mathbf{Z}_{y,i}^{min} \leq \mathbf{Z}_{y,i} \leq \mathbf{Z}_{y,i}^{max}, \quad (18)$$

where $\mathbf{U}_{x,i} = [\dddot{x}_i, \dddot{x}_{i+1}, \ldots, \dddot{x}_{i+N-2}, \dddot{x}_{i+N-1}]^T$ and $\mathbf{U}_{y,i} = [\dddot{y}_i, \dddot{y}_{i+1}, \ldots, \dddot{y}_{i+N-2}, \dddot{y}_{i+N-1}]^T$ denotes the size of N of the CoM jerk vector in the x- and y- directions, respectively. $Z_{x,i}^{min}$, $Z_{x,i}^{max}$, $Z_{y,i}^{min}$ and $Z_{y,i}^{max}$ denote minimum and maximum boundary of ZMP constraints in $x-$ and $y-$ directions, respectively. α_x, β_x, and γ_x are the gains from minimizing the ZMP error, CoM velocity fluctuation and CoM jerk in the $x-$ direction, respectively. And α_y, β_y, and γ_y are the gains in the $y-$ direction. A CoM trajectory in $x-$ direction in generated using (12) and the first value of $\mathbf{U}_{x,i}$ in (18). The CoM trajectory in $y-$ direction is generated using (13) and $\mathbf{U}_{y,i}$.

B. PELVIS TRAJECTORY GENERATION

The position trajectory of the pelvis frame that is used as the base frame of the robot is created to track the CoM trajectory.

$$\mathbf{X}_{pel,i+1} = \mathbf{X}_{pel,i} + K_p(\mathbf{X}_{c,i}^d - \mathbf{X}_{c,i}^m), \quad (19)$$

where $\mathbf{X}_{pel,i} \in \mathbb{R}^3$ is the desired pelvis position at discrete time i, and $\mathbf{X}_{c,i}^d$ and $\mathbf{X}_{c,i}^m$ are desired and measured positions of the CoM at discrete time i, respectively. K_p is the gain. The pelvic-trajectory orientation is zero.

C. FOOT TRAJECTORY GENERATION

In the foot-trajectory generation, the trajectories of the supporting foot and the swing foot are generated separately. The trajectory of the supporting foot is attached to the ground; therefore, the velocity trajectories of the position and orientation are designed to be zero.

$$\dot{\mathbf{x}}_{sp} = 0, \quad (20)$$

where $\mathbf{x}_{sp} \in \mathbb{R}^6$ comprises x, y, z, ϕ, θ, and ψ.

The swing-foot trajectory is generated using a cubic function such that the position and velocity are continuous, and the swing foot can then pass the predetermined foothold.

$$\mathbf{x}_{sw}(t) = a_1 + a_2 t + a_3 t^2 + a_4 t^3. \quad (21)$$

Each coefficient is set to satisfy initial and terminal conditions: $\mathbf{x}_{sw}(t_0) = P_{k-1}^f$, $\mathbf{x}_{sw}(t_f) = P_{k+1}^f$, $\dot{\mathbf{x}}_{sw}(t_0) = \dot{\mathbf{x}}_{sw}(t_f) = 0$. t_0 and t_f are the initial and final times of the step, respectively. P_{k-1}^f denotes the position of the prior support foot. P_{k+1}^f is the position of the next support foot and the landing position of the swing foot. The desired velocity trajectory of the swing foot is created using (21).

D. CHANGING THE FRAME OF THE WALKING PATTERN

Humanoid robots are characterized by floating base. To control a robot with a floating base, the position and velocity of the floating base frame expressed are estimated in the global frame, and each end-effector expressed in the base frame is then controlled. In this study, it is assumed that the floating base, global, and pelvis frames have the same coordinates. The pelvis and foot trajectories generated based on the supporting-foot frame in the previous section are changed to the pelvis-frame coordinates:

$$^p\dot{\mathbf{X}}_{sw} = \,_p^{sp}T^{-1} \cdot \dot{\mathbf{X}}_{sw}, \quad (22)$$
$$^p\dot{\mathbf{X}}_{sp} = \,_p^{sp}T^{-1} \cdot \dot{\mathbf{X}}_{sp}, \quad (23)$$

where $^p\dot{\mathbf{X}}_{sw}$ and $^p\dot{\mathbf{X}}_{sp}$ are the desired swing foot and support foot trajectories represented in the pelvis frame, respectively. $_p^{sp}T^{-1}$ is the transformation matrix that maps the support-foot frame to the pelvis frame.

Equations (22) and (23), which are represented in the pelvis frame, are used together with the lower-body Jacobian, $\mathbf{J}_{low}$ of (9) for IK to obtain the leg-joint angular velocity:

$$\dot{\mathbf{q}}_{low} = \mathbf{J}_{low}^\dagger \,^p\dot{\mathbf{X}}_f, \quad (24)$$

where $J_{low}^\dagger$ is the pseudo inverse-Jacobian of the lower body, and $^p\dot{\mathbf{X}}_f = [^p\dot{\mathbf{X}}_{Lf}, \,^p\dot{\mathbf{X}}_{Rf}]^T$ is the desired foot-velocity vector. $\dot{\mathbf{X}}_{Lf}$ and $\dot{\mathbf{X}}_{Rf}$ are replaced with (22) and (23) depending on whether the foot is a support foot or a swing foot.

V. PROPOSED METHOD FOR OPTIMIZING PELVIC ROTATION TRAJECTORY

This section describes the proposed method for optimizing the pelvic-rotation trajectory using the predicted future state of the CoM in the MPC scheme. With the predicted CoM states and the foot trajectory, which is generated in advance, the angular velocity of the the waist yaw joint is optimized using the MPC. The optimized waist yaw joint is used as the constraint for the QP-based IK to track the desired foot velocity. Centroidal dynamics is used to generate the arm-swing motion to compensate for the yaw angular momentum.

A. PREDICTING FUTURE COM STATE

The CoM jerk, $\mathbf{U}_{x,i}^*$ and $\mathbf{U}_{y,i}^*$, which are optimized in (18), (12), and (13) are used to predict the future COM states, $\hat{\mathbf{X}}_{i+1}$. Equation (12) is recursively used to calculate $\hat{\mathbf{X}}_{i+1}$, and the notation of our previous study [12] is used:

$$\hat{\mathbf{X}}_{i+1} = \mathbf{P}_A\mathbf{x}_i + \mathbf{P}_B\mathbf{U}_{x,i}^*. \quad (25)$$

The predicted future CoM y state, $\hat{\mathbf{Y}}_{i+1}$ is calculated in the same manner as (13) and $\mathbf{U}_{y,i}^*$.

$$\hat{\mathbf{Y}}_{i+1} = \mathbf{P}_A\mathbf{y}_i + \mathbf{P}_B\mathbf{U}_{y,i}^*. \quad (26)$$

Each element of (25) and (26) is used in conjunction with the foot trajectory to predict the future distance between the pelvis and feet at instant time, t_i.

(a) Top view of fixed-pelvis walking

(b) Side view of fixed-pelvis walking
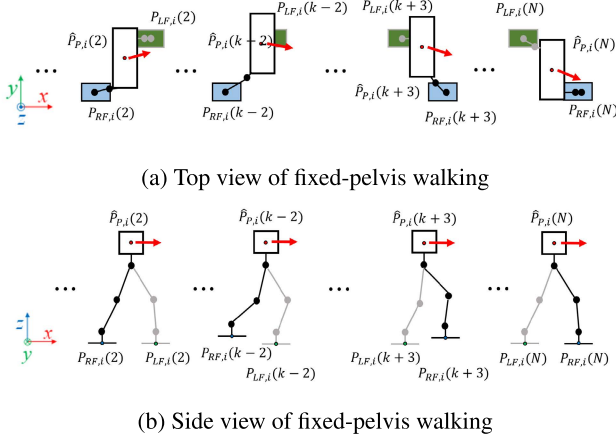
FIGURE 5. The predicted positions of the pelvis and predefined foot trajectory for fixed-pelvis walking for the time horizon at time t_i. In (a), the blue and green rectangles are the right and left feet, respectively. The white rectangle is the pelvis. In (b), the black line and dots denote the right leg as the swinging leg, and the gray line and dots are the left leg as the supporting leg.

(a) Top view of pelvic-rotation walking

(b) Side view of pelvic-rotation walking

FIGURE 6. The predicted position of the pelvis and predefined foot trajectory for pelvic-rotation walking for the time horizon at time t_i. In (a), the rectangle with the gray dot denotes the position of the pelvis without rotation. The black line pelvis is the position of the pelvis with rotation. In the (b), as the pelvis rotates, the $x-$position of the left and right hips are not the same, but move back and forth.

B. DETERMINING REFERENCE PELVIC-ROTATION TRAJECTORY

A reference trajectory for the pelvic rotation angle is required to optimize the pelvic-rotation trajectory using the MPC scheme. To obtain the reference pelvic rotation angle, the robot's pelvis and foot positions for a future time horizon are required. The future position of the foot can be obtained from a predetermined foot trajectory. The future position of the pelvis, $\hat{\mathbf{P}}_{P,i} \in \mathbb{R}^{3 \times N}$, can be predicted using (25) and (26), with the assumption that the position of the pelvis is the same as that of the CoM, and the height of the pelvis is constant.

$$\hat{\mathbf{P}}_{P,i}(k) = \{(\hat{x}_k, \hat{y}_k, z_k) \mid \hat{x}_k \in \hat{\mathbf{X}}_i(k), \hat{y}_k \in \hat{\mathbf{Y}}_i(k), z_k = z_0\}, \tag{27}$$

where k is an instantaneous future time from instant time i, ($k = 1, 2, \ldots N-1, N$). $\hat{x}_k$ and $\hat{y}_k$ are the predicted $x-$ and $y-$ positions of the kth predicted CoM position from instant time i, respectively. z_0 is the constant CoM height. The future positions of the left foot, $\mathbf{P}_{LF,i} \in \mathbb{R}^{3 \times N}$, and the right foot, $\mathbf{P}_{RF,i} \in \mathbb{R}^{3 \times N}$, are obtained from the predefined foot trajectories, as explained in Section IV-C.
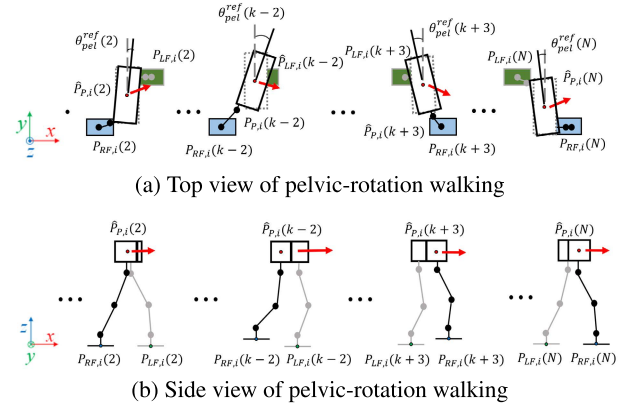
Fig. 5 shows the future robot states predicted for time t_i. If the pelvic orientation is fixed, only the leg joints (hip, knee, and ankle) are used to track the desired foot trajectory. However, if the pelvis rotates, both hip joints are not in a straight line, and are moved back and forth. Pelvic rotation affects the step length by as much as the distance between both hip joints along the $x-$axis, and the distance moved by the legs decreases.

The distance between the pelvis and feet can be calculated using $\hat{\mathbf{P}}_{p,i}$, $P_{RF,i}$ and $P_{LF,i}$:

$$\Delta d_{LFP,i}(k) = \mathbf{P}_{LF,i,x}(k) - \hat{\mathbf{P}}_{P,i,x}(k), \tag{28}$$

$$\Delta d_{RFP,i}(k) = \mathbf{P}_{RF,i,x}(k) - \hat{\mathbf{P}}_{P,i,x}(k), \tag{29}$$

$$(k = 1, 2, \ldots, N-1, N)$$

where $\Delta d_{LFP,i}(k)$ and $\Delta d_{RFP,i}(k)$ are the distances from the pelvis to the left and right feet, respectively. $\mathbf{P}_{LF,i,x}$ and $\mathbf{P}_{RF,i,x}$ are the $x-$positions of left and right feet, respectively. $\hat{\mathbf{P}}_{P,i,x}$ is the predicted $x-$position of the pelvis. The reference pelvic angle is determined such that the step length using pelvic rotation increases in proportion to the distance between the pelvis and the swing foot.

$$\theta_{pel}^{ref}(k) = \frac{\theta_{LFP}(k) + \theta_{RFP}(k)}{2}, \tag{30}$$

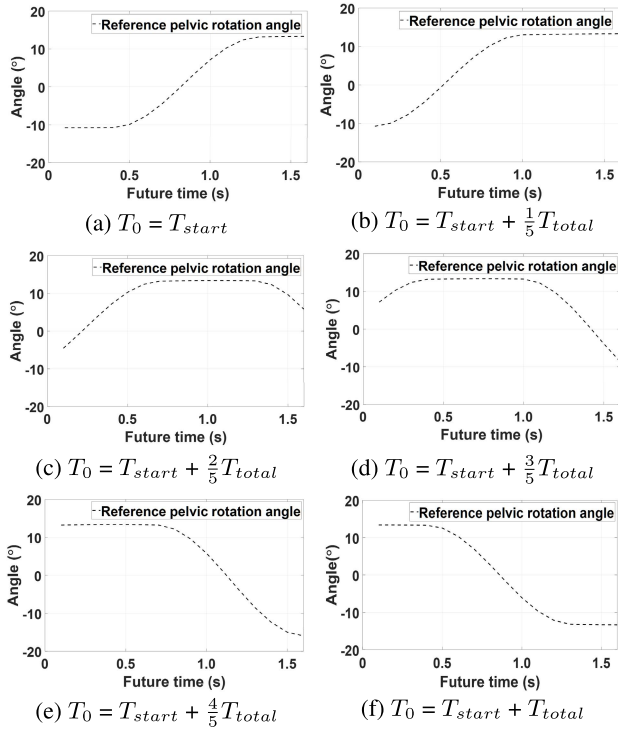$$\theta_{LFP}(k) = tan^{-1}(\frac{k_{pel} \Delta \mathbf{d}_{LFP,i,x}(k)}{\Delta \mathbf{d}_{LFP,i,y}}), \tag{31}$$

$$\theta_{RFP}(k) = tan^{-1}(\frac{k_{pel} \Delta \mathbf{d}_{RFP,i,x}(k)}{\Delta \mathbf{d}_{RFP,i,y}}). \tag{32}$$

where the $\theta_{pel}^{ref}(k)$ denotes the reference pelvic angle based on the predicted kth future robot state at t_i. θ_{LFP} and θ_{RFP} are the angles between the left and right feet and the pelvis, respectively. k_{pel} is the gain that determines the ratio of the moving distance due to the rotation of the pelvis to the total step length. $\Delta \mathbf{d}_{FP,i,x}$ and $\Delta \mathbf{d}_{FP,i,y}$ are the distances from the pelvis to each foot in the $x-$ and $y-$ directions, respectively. As shown in Fig. 6, even with pelvic rotation, the positions of the pelvis and foot did not change. The movement of both leg joints is reduced by the distance between the hip joints caused by pelvic rotation.

A reference pelvic rotation trajectory, Θ_{pel}^{ref}, that can be predicted from t_i is determined using N (30).

$$\Theta_{pel}^{ref} = \begin{bmatrix} \theta_{pel}^{ref}(1) & \theta_{pel}^{ref}(2) & \cdots & \theta_{pel}^{ref}(N-1) & \theta_{pel}^{ref}(N) \end{bmatrix}^T. \tag{33}$$

Fig. 7 shows the predicted reference pelvic-rotation trajectory for every $\frac{1}{5}T_{total}$ in one step. The time at which a step starts is T_{start}, the time required for one step is T_{total}, and the time horizon to predict the pelvic-rotation angle is 1.6 s. As time passes, the reference pelvic-rotation trajectory changes to

(a) $T_0 = T_{start}$

(b) $T_0 = T_{start} + \frac{1}{5}T_{total}$

(c) $T_0 = T_{start} + \frac{2}{5}T_{total}$

(d) $T_0 = T_{start} + \frac{3}{5}T_{total}$

(e) $T_0 = T_{start} + \frac{4}{5}T_{total}$

(f) $T_0 = T_{start} + T_{total}$

FIGURE 7. Predicted reference pelvic rotation trajectory. The start time, T_0 is different for each subfigure, and the future time is 1.6 s from the each start time.

reflect the future viewpoint of the robot. The predicted reference pelvic-rotation trajectory is used in the MPC to optimize the angular velocity of the waist yaw joint.

C. PELVIC ROTATION OPTIMIZATION USING MPC

The waist yaw joint angular velocity of the rotating the pelvis is optimized using the MPC with a reference pelvic-rotation trajectory, shown in (33).

To determine the future state of the pelvic rotation, the angle and angular velocity of the pelvis are modelled as follows:

$$\bar{\boldsymbol{\theta}}_{i+1} = \begin{bmatrix} \theta_{i+1} \\ \dot{\theta}_{i+1} \end{bmatrix} = \underbrace{\begin{bmatrix} 1 & \delta t \\ 0 & 1 \end{bmatrix}}_{A_\theta} \begin{bmatrix} \theta_i \\ \dot{\theta}_i \end{bmatrix} + \underbrace{\begin{bmatrix} \frac{1}{2}\delta t^2 \\ \delta t \end{bmatrix}}_{B_\theta} \ddot{\theta}_i. \quad (34)$$
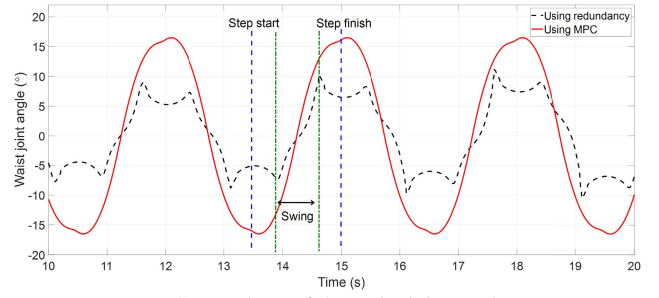
Equation (34) is successively calculated to define a vector consisting of N future states of the pelvic rotation.

$$\boldsymbol{\Theta}_{i+1} = \begin{bmatrix} \bar{\boldsymbol{\theta}}_{i+1} \\ \vdots \\ \bar{\boldsymbol{\theta}}_{i+N} \end{bmatrix} = \mathbf{P}_{A_\Theta}\bar{\boldsymbol{\theta}}_i + \mathbf{P}_{B_\Theta}\ddot{\boldsymbol{\Theta}}_i \quad (35)$$

where,

$$\ddot{\boldsymbol{\Theta}}_i = \begin{bmatrix} \ddot{\theta}_i & \ddot{\theta}_{i+1} & \cdots & \ddot{\theta}_{i+N-2} & \ddot{\theta}_{i+N-1} \end{bmatrix}^T, \quad (36)$$
$$\mathbf{P}_{A_\Theta} = \begin{bmatrix} \mathbf{A}_\theta^T, & (\mathbf{A}_\theta^2)^T, & \cdots, & (\mathbf{A}_\theta^{N-1})^T, & (\mathbf{A}_\theta^N)^T \end{bmatrix},$$

(a) Comparison of the waist joint angle.
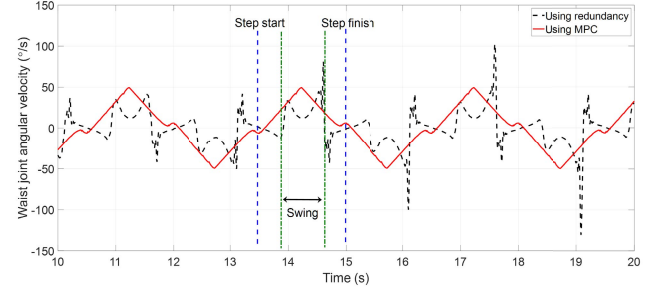
(b) Comparison of the waist joint angular velocity.

FIGURE 8. Comparison of the methods used to generate the waist yaw joint pattern when the step length is 0.3 m.

$$\mathbf{P}_{B_\Theta} = \begin{bmatrix} \mathbf{B}_\theta & 0 & \cdots & 0 & 0 \\ \mathbf{A}_\theta\mathbf{B}_\theta & \mathbf{B}_\theta & \cdots & 0 & 0 \\ \vdots & \vdots & \ddots & \vdots & \vdots \\ \mathbf{A}_\theta^{N-2}\mathbf{B}_\theta & \mathbf{A}_\theta^{N-3}\mathbf{B}_\theta & \cdots & \mathbf{B}_\theta & 0 \\ \mathbf{A}_\theta^{N-1}\mathbf{B}_\theta & \mathbf{A}_\theta^{N-2}\mathbf{B}_\theta & \cdots & \mathbf{A}_\theta\mathbf{B}_\theta & \mathbf{B}_\theta \end{bmatrix}$$

The cost function of the MPC that is used to obtain the pelvic rotation trajectory is defined to minimize the error of the reference pelvic-rotation angle, $\boldsymbol{\Theta}_{i+1}^{ref}$, and the control input, $\ddot{\boldsymbol{\Theta}}_i$.

$$\min_{\ddot{\boldsymbol{\Theta}}_i} \frac{\alpha_{pel}}{2}\|\boldsymbol{\Theta}_{pel,i+1}^{ref} - \boldsymbol{\Theta}_{angle,i+1}\|^2 + \frac{\beta_{pel}}{2}\|\ddot{\boldsymbol{\Theta}}_i\|^2$$
$$\text{s. t. } \boldsymbol{\Theta}_{angle,min} \le \boldsymbol{\Theta}_{angle,i+1} \le \boldsymbol{\Theta}_{angle,max}, \quad (37)$$

where $\boldsymbol{\Theta}_{angle,i+1}$ is the pelvic rotation angle vector in (35). The minimum and maximum angles of the constraints, $\boldsymbol{\Theta}_{angle,min}$ and $\boldsymbol{\Theta}_{angle,max}$ are determined based on the kinematic information of the robot. Using the first value of the $\ddot{\boldsymbol{\Theta}}_i$ optimized in (37), $\bar{\boldsymbol{\theta}}_{i+1}$ is updated, and $\dot{\theta}_{i+1}$ is used as a constraint in the next optimal layer, which is the QP-based IK for walking:

$$\bar{\boldsymbol{\theta}}_{i+1} = \mathbf{A}_\theta\bar{\boldsymbol{\theta}}_i + \mathbf{B}_\theta\ddot{\boldsymbol{\Theta}}_i(0). \quad (38)$$

The angle and angular velocity of the waist yaw joint generated in (38) and that of using redundancy [21] are compared in Fig. 8. As shown in Fig. 8(a), the angle of the waist yaw joint generated using redundancy rotates according to the movement of the swinging leg in the swinging section. However, in the non-swinging DSP, the waist joint angle decreases toward zero. In addition, as shown in Fig. 8(b), the angular velocity of the waist yaw joint
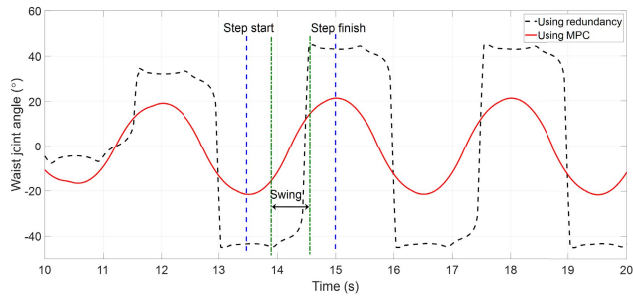
(a) Comparison of the waist joint angle.
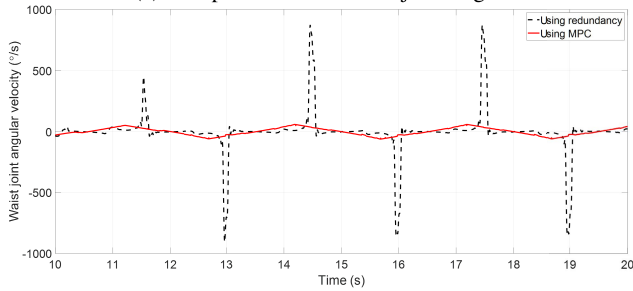
(b) Comparison of the waist joint angular velocity.

FIGURE 9. Comparison of the methods used to generate the waist yaw joint pattern when the step length is 0.4 m.

also changes before and after the swing starts; therefore, the acceleration is expected to be large. However, Fig. 8(a) shows that the waist yaw joint angle generated by the proposed method is smoothly generated from the moment the step starts to the moment the step ends. Fig. 8(b) shows that there is no section in which the joint angular velocity generated using the proposed method changes rapidly.

Fig. 9 shows that the difference between the angle and angular velocity based on the method used to optimize the waist joint angle becomes larger when the step length is increased. Fig. 9(a) shows that the pelvic-rotation angle that is optimized using MPC is smoothly generated in a similar manner to a sine function from $-22°$ at the beginning of the step to $22°$ at the end of the step. When generating pelvic rotation using MPC, the positions of the pelvis and foot of the robot in the future are reflected, and the waist yaw joint rotates in advance before the swing starts. However, in the method using redundancy, the pelvic rotation angle does not change during the DSP. The waist yaw joint starts to rotate when the foot of the robot starts swinging and rotates rapidly in a short time. This may impair the robot's walking stability. However, in the proposed method using MPC, the angular velocity does not change rapidly.

D. QUADRATIC PROGRAMMING-BASED IK FOR WALKING

This section describes the QP-based IK method used to calculate the angular velocity of the leg joints to track the desired foot trajectory. An optimized waist-joint angular velocity is used as a constraint such that the robot tracks the desired foot

trajectory while the pelvis rotates.

$$
\min_{\dot{\mathbf{q}}_{low}} \quad \frac{1}{2} \| \mathbf{J}_{low} \cdot \dot{\mathbf{q}}_{low} - {}^{P}\dot{\mathbf{X}}_{f,d} \|^2
$$

$$
\text{s.t.} \quad \dot{q}_{wy} = \dot{\theta}_{i+1},
$$

$$
\times \frac{\mathbf{q}_{low,min} - \mathbf{q}_{low,cur}}{\Delta t} \le \dot{\mathbf{q}}_{low} \le \frac{\mathbf{q}_{low,max} - \mathbf{q}_{low,cur}}{\Delta t},
$$

$$
\times \dot{\mathbf{q}}_{low,min} \le \dot{\mathbf{q}}_{low} \le \dot{\mathbf{q}}_{low,max}, \tag{39}
$$

where the $\mathbf{q}_{low,min}$ and $\mathbf{q}_{low,max}$ are the minimum and maximum joint angle limitation of lower body, respectively. $\mathbf{q}_{low,cur}$ is the current joint angle of the lower body, and Δt is control period. The value of $\dot{\theta}_{i+1}$ for the first constraint is the optimized joint angular velocity from (34)-(37). The second and third constraints are the joint angle and joint angular velocity constraints, respectively.

The joint angle is input to a position-controlled robot; therefore, the desired joint angle, $\dot{\mathbf{q}}_{low,d}$ is calculated using $\mathbf{q}_{low}^*$, which was optimized in (39):

$$
\mathbf{q}_{low,d} = \mathbf{q}_{low,cur} + \Delta t \cdot \dot{\mathbf{q}}_{low}^*. \tag{40}
$$

E. COMPENSATION OF YAW ANGULAR MOMENTUM USING CENTROIDAL DYNAMICS

The yaw angular momentum generated when the robot walks with a long step can cause instability by increasing the robot's angular momentum. To compensate the yaw angular momentum, the upper-body motion is generated using centroidal dynamics [17]. The yaw angular momentum values of the upper body and lower body are calculated using the respective centroidal momentum matrix and joint angular velocity.

$$
h_{low}^{yaw} = \mathbf{A}_{low,yaw}^{CMM} \cdot \dot{\mathbf{q}}_{low}, \tag{41}
$$

$$
h_{up}^{yaw} = \mathbf{A}_{up,yaw}^{CMM} \cdot \dot{\mathbf{q}}_{up}, \tag{42}
$$

where, h_{low}^{yaw} and h_{up}^{yaw} are the yaw angular momentum of the lower body and upper body, respectively. $\mathbf{A}_{low,yaw}^{CMM}$ and $\mathbf{A}_{up,yaw}^{CMM}$ are centroidal yaw angular-momentum matrices for the lower body and upper body, respectively. Because $\mathbf{q}_{low,d}$ in (40) is used in (41), h_{low}^{yaw} is the yaw angular momentum that will occur owing to the movement of the lower body. When $h_{low}^{yaw} + h_{up}^{yaw} \simeq 0$, h_{low}^{yaw} caused by the lower body is compensated, and the value of $\dot{\mathbf{q}}_{up}$ used to generate h_{up}^{yaw} is optimized as follows:

$$
\min_{\dot{\mathbf{q}}_{up}} \quad \frac{\omega_1}{2} \| h_{low}^{yaw} + h_{up}^{yaw} \|^2 + \frac{\omega_2}{2} \| \mathbf{q}_{up}^{init} - \mathbf{q}_{up} \|^2 + \frac{\omega_3}{2} \| \dot{\mathbf{q}}_{up} \|^2
$$

$$
\text{s.t.} \quad \frac{\mathbf{q}_{up,min} - \mathbf{q}_{up,cur}}{\Delta t} \le \dot{\mathbf{q}}_{up} \le \frac{\mathbf{q}_{up,max} - \mathbf{q}_{up,cur}}{\Delta t}
$$

$$
\times \dot{\mathbf{q}}_{up,min} \le \dot{\mathbf{q}}_{up} \le \dot{\mathbf{q}}_{up,max}, \tag{43}
$$

where, ω_1, ω_2, and ω_3 are weighting coefficients for each cost function, respectively. The $\mathbf{q}_{up}^{init}$ is the joint angle of the initial pose of the upper body. $\mathbf{q}_{up,min}$ and $\mathbf{q}_{up,max}$ are the minimum and maximum limitations of the upper body joint, respectively. $\mathbf{q}_{up,cur}$ and $\dot{\mathbf{q}}_{up}$ are current joint angle and joint angular velocity of the upper body, respectively. The first

FIGURE 10. Snapshot of the walking with a step length of 0.4 m using the proposed method in the simulation.

term of the cost function in (43) minimizes the yaw angular momentum of the robot. The second term minimizes the error with the initial pose of the robot to prevent the robot from drifting, and the last term serves as a regularization of the upper body joints. The constraints are the joint angle and joint angular velocity constraints.

VI. ANALYSIS OF SIMULATION AND EXPERIMENT

A. SYSTEM SETUP

The method proposed in this study was analyzed using a simulation and then verified experimentally. The humanoid robot Dyros-Jet was used [22] to verify the proposed method. The time horizon of (37) is 1.6 s. In (37), α_{pel}, and β_{pel} are 1 and 10^{-10}, respectively. The weighting factors in (43), ω_1, ω_2, and ω_3, are 1, 10^{-2}, and 10^{-4}, respectively. The shoulder pitch and elbow joints of each arm are used in (43): $\dot{\mathbf{q}}_{up} = [\dot{q}_{L,shoulder}, \dot{q}_{L,elbow}, \dot{q}_{R,shoulder}, \dot{q}_{R,elbow}]^T$. Seventeen DoF joints were used in the simulation. The QP formulae of (37), (39), and (43) were solved using QPOASES [23] at 200 Hz. The computer unit used in the simulation consisted of an Intel (R) Core i7-7770 3.6 GHz processor, 16GB RAM, and an NVIDIA GeForce GTX 1050. To analyze the proposed method, the simulation compared the robot walking without pelvic rotation to walking with pelvic rotation using the redundancy of the lower body [21].

B. INCREASE IN STEP LENGTH

The increase in step length that occurred during pelvic-rotation walking Was compared in the simulation. Three methods were used to compare the increase in step length: walking without pelvic rotation, walking with pelvic rotation using redundancy, and walking with pelvic rotation using the proposed method. Fig. 10 shows the robot walking with pelvic rotation using the MPC. The pelvic-rotation angle and angular velocity generated by the simulation are shown in Figs. 8 and 9.

In the simulation, walking without pelvic rotation was possible up to a a step length of 0.3 m, and walking with pelvic rotation was possible up to 0.4 m. Each possible maximum step length was similar to the value analyzed in Section II. ($l_{stepmax}^{*pelvic-fixed} = 0.31$ m and $l_{stepmax}^{*pelvic-rotation} = 0.42$ m).

Fig. 11 shows the side view of the robot walking with a 0.3 m step length using the proposed method. In Fig. 11, the robot's walking proceeds from left to right, and the two black dots and two donut shapes show the hip position of the supporting and swinging leg when the step starts and ends, respectively. The position of the hip on the supporting leg is
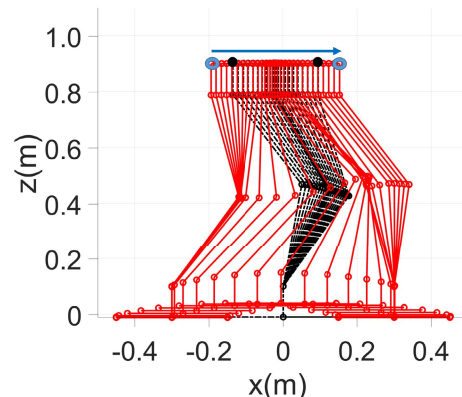
FIGURE 11. Stick diagram of a walking robot during one step using the proposed method. The red lines denote the link between the right leg and foot. The black dotted lines are the link between the left leg and foot. The left leg is the supporting leg, and the right leg is the swinging leg. The black circles on the left and right are the start position and finish positions of the hip of the supporting leg, respectively. The blue circles on the left and right are the start and finish positions of the hip of the swinging leg, respectively.
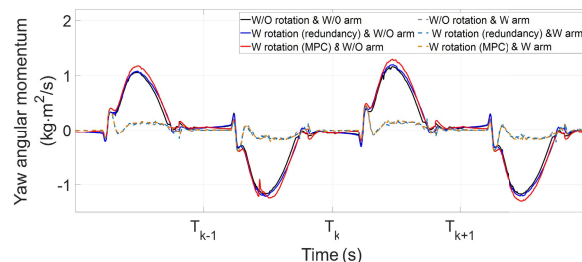
(a) Comparison of yaw angular momentum with step length of 0.3 m.
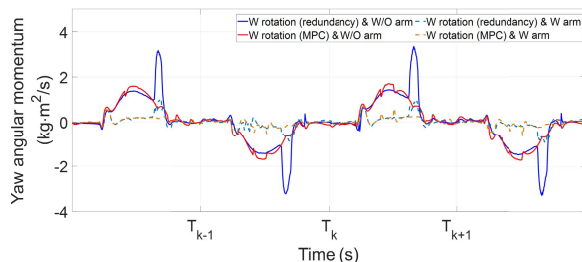
(b) Comparison of yaw angular momentum with step length of 0.4 m.

FIGURE 12. Comparison of the yaw angular momentum for the walking methods with and without arm swing. T_k in the x-axis denotes the time when the kth step starts. The figure compares walking without pelvic rotation (W/O rotation), walking with pelvic rotation using redundancy (W rotation (redundancy)), and walking with pelvic rotation using the proposed method (W rotation (MPC)). The yaw angular momentum with arm swing (W arm) and without arm swing (W/O arm) are compared.

in front of the hip on the swinging leg when the step starts. Because the pelvis rotates when the leg swings, the position of the hip on the swinging leg at the end of the step is ahead of that of the pelvis on the supporting leg.

C. COMPENSATION OF YAW ANGULAR MOMENTUM

The values of the yaw angular momentum generated according to each walking method were compared. As shown in Fig. 12, the simulation verified that the arm swing compensated for the yaw angular momentum. Fig. 12(a) compares

TABLE 1. Comparison of energy consumption during two steps. A total of 100 datapoints are used for each case.

Step length	Walking without pelvic rotation		Walking with pelvic rotation using redundancy		Walking with pelvic rotation using MPC	
	Mean (W)	Standard deviation	Mean (W)	Standard deviation	Mean (W)	Standard deviation
0.15	14.78	2.89	12.79	3.04	10.06	0.87
0.2	19.11	5.55	18.17	6.12	16.92	3.31
0.25	19.76	10.23	27.14	9.16	26.53	2.57
0.3	50.16	22.32	60.49	28.55	157.92	9.73
0.35	—-	——	411.25	208.41	309.64	32.51
0.4	——	——	941.32	597.6	412.34	34.15

the yaw angular momentum values generated according to the walking methods with and without pelvic rotation with a step length of 0.3 m, and the difference does not appear to be significant. This is because that the momentum generated by the pelvic rotation is small compared to that generated by the swinging leg. When arm swing was used for each method, the yaw angular momentum was significantly reduced. Fig. 12(b) shows a comparison of the yaw angular momentum values for a step length of 0.4 m. Compared to the method using MPC, in the method that uses redundancy to generate pelvic rotation, the yaw angular momentum changes rapidly after half the time taken for each step. The time at which the yaw angular momentum changes rapidly is the time at which the robot's leg lands. Because the future state of the robot was not reflected in the method that uses redundancy, the pelvis could not rotate in advance, and the yaw angular momentum was high because the pelvis rotated rapidly before landing. In both methods, the yaw angular momentum was compensated when the arm swing motion was used.

D. ENERGY CONSUMPTION
The energy consumption of each method is compared in this section. The energy consumed during two steps was calculated to compare the energy consumption reflecting the swing of the left and right legs:

$$E_{con} = \sum_{i=1}^{n} \int_{t_s}^{2t_f} max(\tau_i \dot{q}_i \Delta t, 0), \qquad (44)$$

where E_{con} is the energy consumption of the robot during the two steps. t_s and t_f are the step start and finish times, respectively, and n is the number of joints used ($n = 17$). τ_i and $\dot{q}_i$ are the torque and angular velocity of joint i, respectively. The $max(a, 0)$ function returns a if a is greater than 0, and returns 0 if a is less than 0. A negative $\tau_i \dot{q}_i$ value indicates that the energy is stored in the motor. Only a positive $\tau_i \dot{q}_i$ value is reflected in (44) to ensure that only the energy consumed by the motor is compared. The energy consumed by the arm swing was also included; however, the energy consumed by the joints of the arm was small compared with the energy consumed by the leg. This is because the weight of the arm is smaller than that of the leg; therefore, the torque required at the joint of the arm is small. In addition, the value of $\tau_i \dot{q}_i$ calculated at the joints of the arm was typically negative; thus, it was often excluded from E_{con}.

Table 1 shows the average and standard deviation values of the energy consumed during two steps, with step lengths from 0.15 m to 0.4 m. In ten repeated simulations, the energy consumed in 20 steps was measured for each method. The average and standard deviation values of the energy consumed in two steps were obtained (100 datapoints are used for each step length). Because the angle of the waist joint is not considerably large up to a step length of 0.2 m, the energy consumed when walking with a pelvic rotation is smaller than that when walking without it. However, the angle of the pelvic rotation increased when the step length was larger than 0.2 m; therefore, the energy consumed when walking using pelvic rotation was greater than that when walking without it. When walking with pelvic rotation, the method using redundancy consumed more energy than the method using MPC, except for the case of a 0.3 m step length. The standard deviation of the energy consumption was smaller for the MPC method than the redundancy method, and the difference in the standard deviation increased as the step length increased. Thus, it can be observed that the MPC method generates a relatively consistent trajectory every time the walking is repeated, compared with the redundancy method.

E. POSSIBILITY OF SINGULARITY OCCURRENCE
The possible step length when walking with pelvic rotation is 0.1 m longer than that when walking without pelvic rotation. When pelvic rotation was used, the robot's foot was able to reach a position that it could not reach during landing when pelvic rotation was not used. That is, the possibility of the singularity occurrence when walking using pelvic rotation is less than that of walking without pelvic rotation. The possibility of the singularity occurrence can be compared using the condition number, $\kappa(J)$ [24]–[26]:
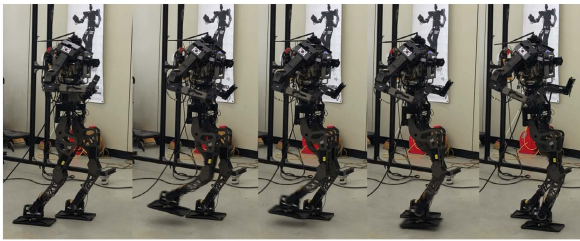
$$\kappa(J) = \frac{\sigma_{max}}{\sigma_{min}}, \qquad (45)$$

where J is the Jacobian matrix of the lower body, and σ_{max} and σ_{min} are the maximum and minimum eigenvalues of the lower-body Jacobian matrix, respectively. As the robot approaches singularity, σ_{min} approaches 0, and $\kappa(J)$ diverges.

Fig. 13 shows the $\kappa(J)$ for one step for each method. When the foot lands at a 0.3 m step length without using pelvic rotation, $\kappa(J)$ is almost double that of the same step length using pelvic rotation. For a 0.35 m step, the $\kappa(J)$ values were significantly increased when the foot lifted for
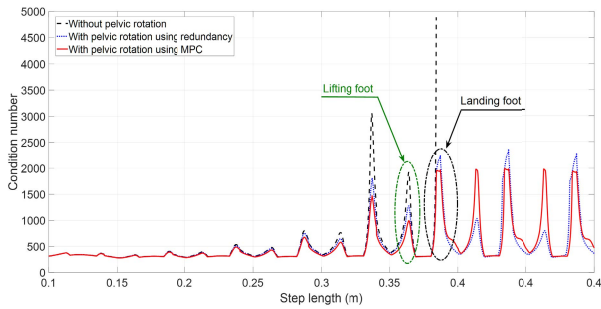
**FIGURE 13.** Comparison of condition number for one step for each method.

FIGURE 14. Photographs of the experiment using the proposed method.

FIGURE 15. Desired and measured CoM trajectory and calculated ZMP trajectory of the proposed pelvic-rotation walking in the experiment. The rectangles are the footholds.

FIGURE 16. Comparison of yaw angular momentum with and without arm motion. The black and red lines are the yaw angular momentum without arm motion and with arm motion, respectively.

all three methods compared to those for a 0.3 m step length. The $\kappa(J)$ value obtained when walking without pelvic rotation was close to twice that of walking with pelvic rotation. When walking without pelvic rotation with a step length of 0.35 m, the robot's foot cannot reach the target point when the foot lands; therefore, a singularity occurs and $\kappa(J)$ diverges. However, pelvic rotation increases the step length such that the foot can reach the foot hold. Therefore, $\kappa(J)$ increased; however, it did not diverge because the singularity did not occur. For a step length of 0.4 m, $\kappa(J)$ increases when foot lifts or lands. During the landing of the foot, the redundancy method produced a $\kappa(J)$ value that was somewhat larger than that of the MPC method; for the lifting of the foot, the MPC method had a larger $\kappa(J)$ value. For pelvic rotation walking using redundancy, the pelvis starts to rotate when the foot swings, and it maintains a large angle of pelvic rotation in the DSP. Therefore, a singularity is less likely to occur before the foot lifts. However, for pelvic rotation using the proposed method, the pelvis rotates during DSP. As the forward distance between the ankle and the hip of the hind leg increased, the possibility of a singularity increased. However, a smaller peak value is preferred; thus, the possibility of a singularity is smaller when MPC is used.

F. EXPERIMENT

The proposed method was verified experimentally. The system setup of the experiment was the same as that of the simulation, except for the computer specifications. The computer unit of the robot used in the experiment consisted of an Intel (R) Core (TM) i7-4770k 3.6 GHz processor, 8GB RAM, and a mini-ITX-size motherboard. Fig. 14 shows photographs of the proposed pelvic rotation walking using MPC. Dyros-Jet could walk with a maximum step length of 0.3 m per 1.2 s in the experiment. The robot started walking at 0.1 m per
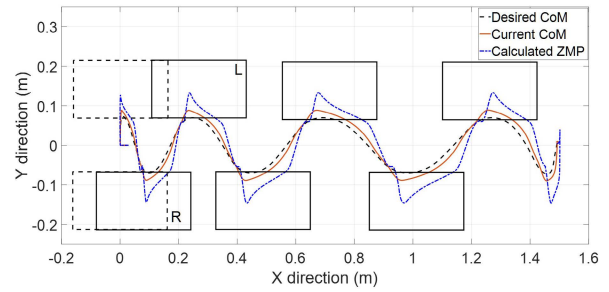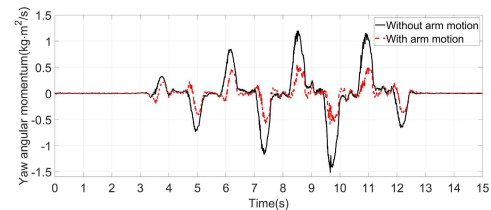
1.2 s; it then increased its step by 0.05 m, and walked with a maximum step length of 0.3 m.

The stability of the pelvic-rotation walking was verified by demonstrating that a ZMP exists in the support polygon. Fig. 15 shows the desired and measured CoM trajectories and the calculated ZMP with the footholds in the experiment. The ZMP was calculated using the measured CoM and the LIPM. The rotation of the pelvis was not considered when generating the CoM trajectory using LIPM; however, Fig. 15 shows that the ZMP exists in the support foot.

As the step length of the robot increased, the yaw angular momentum generated by the swing increased. Unintended yaw angular momentum can weaken the walking stability of the robot and the upper body motion to compensate for this yaw angular momentum is generated from (43).

Fig. 16 shows that the upper-body motion compensated the yaw angular momentum in the experiment. The angular momentum decreased by up to 60% when the upper body was used.

VII. CONCLUSION

This study proposed a method to optimize pelvic-rotation walking using MPC in multilayered optimal control. The multilayered optimal control proposed herein consisted of three layers that optimized the waist yaw joint, leg joints, and upper joints, respectively. The waist yaw joint was optimized using MPC for pelvic-rotation walking. Moreover, the reference pelvis angle used for the MPC was determined using the predicted future positions of the pelvis and foot of the robot. In successive optimal control layers, the leg and upper body joints were optimized to track the desired foot trajectory and compensate the angular momentum. The proposed method was analyzed via a simulation. Walking using pelvic rotation increased the step length by approximately 33% compared

to walking without pelvic rotation. In addition, the pelvic-rotation trajectory generated by reflecting the future state of the robot using MPC was more stable than that generated by reflecting only the robot state at every control time using the redundancy of the robot. The energy consumption of the different walking methods was compared and analyzed in the simulation. Walking using the proposed method consumes the least energy, except for a specific step length. In addition, a comparison of condition numbers showed that walking using pelvic rotation reduces the possibility of a singularity occurrence. The experiment verified the proposed algorithm and demonstrated that the arm swing compensated the yaw angular momentum. In future, we intend to study the utilization of pelvic rotation when changing the position of the foot or changing the CoM trajectory to balance against disturbances. This study considered only the yaw rotation of the pelvis; therefore, we will study the roll and pitch orientation of the pelvis to the robot and analyze its effect. In addition, we will apply the heel-strike and toe-off motions to the robot walking motion to increase the step length by avoiding the singularity that occurs in the hind leg while the robot moves forward during the DSP.

REFERENCES

[1] S. Zhang, Q. Huang, H. Wang, W. Xu, G. Ma, Y. Liu, and Z. Yu, "The mechanism of yaw torque compensation in the human and motion design for humanoid robots," *Int. J. Adv. Robotic Syst.*, vol. 10, no. 1, p. 57, Jan. 2013.

[2] W. Zhang, Q. Huang, Z. Yu, G. Huang, X. Chen, J. Li, G. Ma, L. Meng, Y. Liu, S. Zhang, W. Zhang, and J. Gao, "Human-like walking patterns with pelvic rotation for a humanoid robot," in *Proc. 11th World Congr. Intell. Control Autom.*, Jun. 2014, pp. 1887–1892.

[3] H. Herr and M. Popovic, "Angular momentum in human walking," *J. Experim. Biol.*, vol. 211, no. 4, pp. 467–481, Feb. 2008.

[4] S. H. Collins, P. Adamczyk, and D. Kuo, "Dynamic arm swinging in human walking," *Proc. Roy. Soc. B, Biol. Sci.*, vol. 276, pp. 3679–3688, Oct. 2009.

[5] C. Zhou, X. Wang, Z. Li, D. Caldwell, and N. Tsagarakis, "Exploiting the redundancy for humanoid robots to dynamically step over a large obstacle," in *Proc. IEEE/RSJ Int. Conf. Intell. Robots Syst. (IROS)*, Sep. 2015, pp. 1599–1604.

[6] J. Lim, I. Lee, I. Shim, H. Jung, H. M. Joe, H. Bae, O. Sim, J. Oh, T. Jung, S. Shin, and K. Joo, "Robot system of DRC-HUBO+ and control strategy of team KAIST in DARPA robotics challenge finals," *J. Field Robot.*, vol. 34, no. 4, pp. 802–829, 2017.

[7] H. Takemura, A. Matsuyama, J. Ueda, Y. Matsumoto, H. Mizoguchi, and T. Ogasawarahi, "Momentum compensation for the dynamic walk of humanoids based on the optimal pelvic rotation," in *Climbing and Walking Robots*. Berlin, Germany: Springer, 2006, pp. 485–492.

[8] Z. Huang, Z. Wang, J. Wei, J. Yu, Y. Zhou, P. Lao, X. Huang, X. Zhang, and Y. Zhang, "Three-dimensional posture optimization for biped robot stepping over large ditch based on a ducted-fan propulsion system," in *Proc. IEEE/RSJ Int. Conf. Intell. Robots Syst.*, Oct. 2020, pp. 3591–3597.

[9] S. Kajita, F. Kanehiro, K. Kaneko, K. Fujiwara, K. Harada, K. Yokoi, and H. Hirukawa, "Biped walking pattern generation by using preview control of zero-moment point," in *Proc. IEEE Int. Conf. Robot. Autom.*, vol. 2, Sep. 2003, pp. 1620–1626.

[10] P.-B. Wieber, "Trajectory free linear model predictive control for stable walking in the presence of strong perturbations," in *Proc. 6th IEEE-RAS Int. Conf. Humanoid Robots*, Dec. 2006, pp. 137–142.

[11] A. Herdt, H. Diedam, P.-B. Wieber, D. Dimitrov, K. Mombaur, and M. Diehl, "Online walking motion generation with automatic footstep placement," *Adv. Robot.*, vol. 24, nos. 5–6, pp. 719–737, 2010.

[12] B. Park and J. Park, "Walking pattern generation using MPC with minimization of COM velocity fluctuation," in *Proc. 20th Int. Conf. Control, Autom. Syst. (ICCAS)*, Oct. 2020, pp. 268–273.

[13] B. Ugurlu, J. A. Saglia, N. G. Tsagarakis, and D. G. Caldwell, "Yaw moment compensation for bipedal robots via intrinsic angular momentum constraint," *Int. J. Humanoid Robot.*, vol. 9, no. 4, Dec. 2012, Art. no. 1250033.

[14] H.-O. Lim, S.-H. Hyon, S. A. Setiawan, and A. Takanishi, "Quasi-human biped walking," *Robotica*, vol. 24, no. 2, p. 257, 2006.

[15] J. I. Yamaguchi, E. Soga, S. Inoue, and A. Takanishi, "Development of a bipedal humanoid robot-control method of whole body cooperative dynamic biped walking," in *Proc. IEEE Int. Conf. Robot. Autom.*, vol. 1, May 1999, pp. 368–374.

[16] J. Ueda, K. Shirase, Y. Matsumoto, S. Oda, and T. Ogasawara, "Momentum compensation for fast dynamic walking of humanoids based on pelvic rotation of contact sport athletes," in *Proc. 4th IEEE/RAS Int. Conf. Humanoid Robots*, vol. 2, Nov. 2004, pp. 592–607.

[17] D. E. Orin and A. Goswami, "Centroidal momentum matrix of a humanoid robot: Structure and properties," in *Proc. IEEE/RSJ Int. Conf. Intell. Robots Syst.*, Sep. 2008, pp. 653–659.

[18] D. E. Orin, A. Goswami, and S.-H. Lee, "Centroidal dynamics of a humanoid robot," *Auto. Robot.*, vol. 35, nos. 2–3, pp. 161–176, 2013.

[19] S. Kajita, F. Kanehiro, K. Kaneko, K. Fujiwara, K. Harada, K. Yokoi, and H. Hirukawa, "Resolved momentum control: Humanoid motion planning based on the linear and angular momentum," in *Proc. IEEE/RSJ Int. Conf. Intell. Robots Syst. (IROS)*, vol. 2, Oct. 2003, pp. 1644–1650.

[20] A. Miyata, S. Miyahara, and D. N. Nenchev, "Walking with arm swinging and pelvis rotation generated with the relative angular acceleration," *IEEE Robot. Autom. Lett.*, vol. 5, no. 1, pp. 151–158, Jan. 2020.

[21] B. Park, M.-J. Kim, E. Sung, J. Kim, and J. Park, "Whole-body walking pattern using pelvis-rotation for long stride and arm swing for yaw angular momentum compensation," in *Proc. IEEE-RAS 20th Int. Conf. Humanoid Robots (Humanoids)*, Jul. 2021, pp. 47–52.

[22] S. Park, J. Sim, and J. Park, "System design of humanoid robot DYROS-JET," in *Proc. IEEE/SICE Int. Symp. Syst. Integr. (SII)*, Jan. 2019, pp. 746–750.

[23] H. J. Ferreau, C. Kirches, A. Potschka, H. G. Bock, and M. Diehl, "qpOASES: A parametric active-set algorithm for quadratic programming," *Math. Program. Comput.*, vol. 6, no. 4, pp. 327–363, 2014.

[24] S. Chiaverini, B. Siciliano, and O. Egeland, "Review of the damped least-squares inverse kinematics with experiments on an industrial robot manipulator," *IEEE Trans. Control Syst. Technol.*, vol. 2, no. 2, pp. 123–134, Jun. 1994.

[25] A. Colomé and C. Torras, "Closed-loop inverse kinematics for redundant robots: Comparative assessment and two enhancements," *IEEE/ASME Trans. Mechatronics*, vol. 20, no. 2, pp. 944–955, Apr. 2015.

[26] A. K. Cline, C. B. Moler, G. W. Stewart, and J. H. Wilkinson, "An estimate for the condition number of a matrix," *SIAM J. Numer. Anal.*, vol. 16, no. 2, pp. 368–375, 1979.

BEOMYEONG PARK received the B.S. degree in mechanical engineering from Konkuk University, Seoul, South Korea, in 2013. He is currently pursuing the Ph.D. degree with the Department of Intelligence and Information, Seoul National University, Seoul. His research interests include bipedal locomotion control, whole body motion planning of humanoid robot, and optimal motion planning.

JAEHEUNG PARK (Member, IEEE) received the B.S. and M.S. degrees in aerospace engineering from Seoul National University, South Korea, in 1995 and 1999, respectively, and the Ph.D. degree in aeronautics and astronautics from Stanford University, USA, in 2006. From 2006 to 2009, he was a Postdoctoral Researcher and later a Research Associate with the Stanford Artificial Intelligence Laboratory. From 2007 to 2008, he worked part-time with Hansen Medical Inc., a medical robotics company, USA. Since 2009, he has been a Professor with the Department of Intelligent Convergence Systems, Seoul National University. His research interests include robot-environment interaction, contact force control, robust haptic teleoperation, multicontact control, whole-body dynamic control, biomechanics, and medical robotics.

● ● ●